

Symmetry-Driven Novel Kondo Effect in a Molecule

Emi Minamitani,¹ Noriyuki Tsukahara,² Daisuke Matsunaka,³ Yousoo Kim,¹ Noriaki Takagi,^{2,*} and Maki Kawai²

¹RIKEN, 2-1 Hirosawa, Saitama 351-0198, Japan

²Department of Advanced Materials Science, The University of Tokyo, 5-1-5 Kashiwanoha, Kashiwa, Chiba 277-8561, Japan

³Department of Mechanical Engineering, Osaka University, 2-1 Yamadaoka, Suita, Osaka, Japan

(Received 7 May 2012; published 22 August 2012)

The Kondo effect caused by the adsorption of iron phthalocyanine (FePc) on Au(111) was investigated by the combination of density functional theory and a numerical renormalization group calculation with scanning tunneling microscopy. We found that a novel Kondo effect is realized for a single FePc molecule on Au(111) by tuning the symmetry of the ligand field through the local coordination to the substrate. For FePc in the on top configuration where fourfold symmetry around the Fe²⁺ ion is held, the orbital degrees of freedom survive, resulting in the spin+orbital SU(4) Kondo effect. In contrast, the reduced symmetry in the bridge configuration freezes the orbital degrees of freedom, leading to the spin SU(2) Kondo effect. These results provide a novel example to manipulate the many-body phenomena by tuning the local symmetry.

DOI: [10.1103/PhysRevLett.109.086602](https://doi.org/10.1103/PhysRevLett.109.086602)

PACS numbers: 72.15.Qm, 71.10.-w, 71.15.Mb, 73.20.-r

The Kondo effect is one of the cooperative many-body phenomena in condensed matter physics [1,2]. The spin degree of freedom of the magnetic impurity is coupled with the conduction electrons at the Fermi sea of the reservoir, which causes coherent spin-flip scattering between the impurity spin and the conduction electrons. As a result, the magnetic moment of the impurity spin is collectively screened through the formation of a Kondo resonance state near the Fermi level, E_F , below the Kondo temperature, T_K . The Kondo effect has emerged in diverse systems from dilute-magnetic alloys [1,2] to quantum dots (QDs) [3–6], magnetic atoms [7–10], and molecules [11–17] connected to electronic reservoirs. Most of the Kondo effects are categorized into SU(2) symmetry, reflecting the number of spin degrees of freedom.

Besides the spin, other degrees of freedom can also trigger the Kondo correlations [5,6,18]. The orbital degree of freedom behaves as a pseudospin to bring about the Kondo effect. Furthermore, in the presence of both orbital and spin degrees of freedom, the quantum fluctuations between these degrees of freedom cause an exotic Kondo effect obeying SU(4) symmetry. Since the SU(4) Kondo effect needs robust orbital degeneracy, it has been clearly observed only in the carbon-nanotube QD where an electron has the orbital degrees of freedom derived from the two-dimensional electronic band structure peculiar to graphene [18–20]. Orbital degeneracy commonly occurs in various organic molecules such as metal phthalocyanine, metal porphyrine, etc., and thus the SU(4) Kondo effect should be realized for these molecules by tuning the coupling between the molecules and the electron reservoir. Recent x-ray magnetic circular dichroism work with iron phthalocyanine (FePc) on Au(111) has shown that the orbital degree of freedom survives and the molecule has a sizable in-plane orbital magnetic moment [21]. Thus, we

investigated the possibility of the SU(4) Kondo effect for FePc on Au(111) by *ab initio* calculations based on density functional theory and a numerical renormalization group (NRG) calculation together with scanning tunneling microscopy (STM) and scanning tunneling spectroscopy (STS).

All of the experiments were carried out in an ultrahigh vacuum chamber (base pressure of 5×10^{-11} Torr). All of the STM and STS measurements were made at 0.4 K except for the measurements under magnetic fields where the temperature rose to 0.7 K. The magnetic field dependence of the STS spectrum was measured using two types of superconducting magnets; one provides magnetic fields perpendicular to the sample surface (0–11 T) and the other provides magnetic fields parallel to the surface (0–7 T). *Ab initio* calculations were made based on the density functional theory using the plane wave-based Vienna *ab initio* simulation package (VASP) [22,23] with the projected augmented wave method [24]. To treat the *d*-electron states in the Fe atom, we have employed the LDA + U method with $U = 2.0$ and $J = 1.0$ eV [25–27]. The experimental and calculational details are presented in the Supplemental Material Ref. [28].

The FePc molecule appears as a cross in the STM image [Fig. 1(a)]. The central bright spot is the Fe atom and the four lobes are the aromatic rings. The molecule takes two types of adsorption configurations, i.e., the on top and bridge configurations. In the on top (bridge) configuration, the Fe atom is located in the on top (bridge) site with the molecular plane parallel to the surface. Both species show characteristic spectral features near E_F [Figs. 1(b) and 1(c)]. For the on top species, a broad peak appears accompanied by a sharp dip structure inside the peak. In contrast, only a broad peak is observed for the bridge species. The spectral feature of the on top species is well

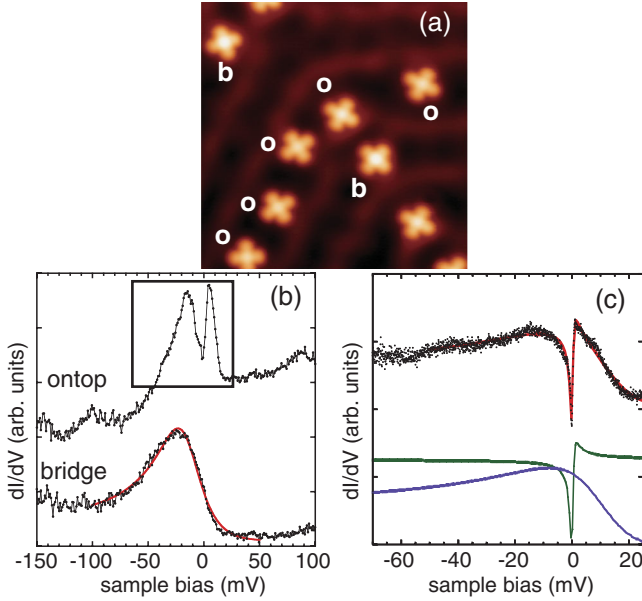


FIG. 1 (color). (a) The topographic STM image of FePc on Au(111) taken at 0.4 K with the tunneling current $I_t = 100$ pA and the sample bias $V_s = -0.1$ V. The image size is $15 \text{ nm} \times 15 \text{ nm}$. The on top and bridge species are specified by o and b , respectively. (b) The STS spectra were taken for both species at 0.4 K by keeping the feedback off, respectively. The spectra were measured by adding the modulation voltage of $V_{\text{rms}} = 2$ mV and 312.6 Hz to V_s and by holding the STM tip over the Fe atom. The red curve for the bridge species is a fit to a Fano function with $q = -3.13$, $\epsilon_0 = -15.2$ meV, and $\Gamma = 24.9$ meV, where q is the Fano asymmetry parameter, ϵ_0 is the energy shift of the resonance from E_F , and Γ is the half-width of the resonance. (c) High-resolution spectrum for the on top species taken with $V_{\text{rms}} = 0.2$ mV and 312.6 Hz in the region marked by a rectangle in (b) [The dip in (b) is broadened by using larger V_{rms}]. The green and purple curves are calculated by Fano functions for the narrow dip ($q = 0.45$, $\epsilon_0 = -0.19$ meV, and $\Gamma = 0.61$ meV) and broad peak ($q = -1.14$, $\epsilon_0 = -9.62$ meV, and $\Gamma = 20.0$ meV). The overall spectral shape is well reproduced by the linear combination (red curve) of the green and purple curves.

reproduced by two Fano functions [8,17,29–31], suggesting that two channels screen the molecular spin. The dip structure reflects the low- T Kondo channel of $T_K = 2.6 \pm 1.4$ K [16], and the broad peak the high- T Kondo channel of $T_K = 110\text{--}150$ K estimated from the width. The broad peak observed for the bridge species is also reproduced by the Fano function and the plausible origin is a Kondo resonance of $T_K = \sim 200$ K.

To gain insight into the origin of the spectral features, the geometric and electronic structures were investigated by LDA + U calculations. Consistent with the STM results, we found that the on top and bridge species are stable [Fig. 2(a)]. Figure 2(b) shows the spin-polarized (SP) local density of states (LDOS) projected on the d_{z^2} and d_{π} (d_{zx} and d_{yz}) orbitals of Fe for both species. The majority and minority spin states are inequivalently occupied for both species, leading to a total spin magnetic moment of

1.61 and $1.45 \mu_B$ for the on top and bridge species, respectively. Therefore, the valence of Fe can be approximately described as Fe^{2+} ($S = 1$) with an electronic configuration of $(d_{xy})^2(d_{z^2})^1(d_{\pi})^3$ similar to that of the isolated and bulk FePc. The main components of d_{z^2} in the LDOS appear as split peaks around $-2 \sim -1$ eV ($-1 \sim +1$ eV) for the majority (minority) spin state common to both species. The d_{zx} and d_{yz} orbitals are observed at -1.5 eV ($+0.1$ eV) for the majority (minority) spin state. The splitting of the d_{z^2} orbital reflects a stronger hybridization with the substrate than those of the d_{π} orbitals. The overall LDOS features of both species are similar to each other, but a marked difference is observed for the d_{π} orbitals. The peaks of the d_{zx} and d_{yz} orbitals of the on top species overlap each other whereas they are separated by 100 meV for the bridge species. The degeneracy in the

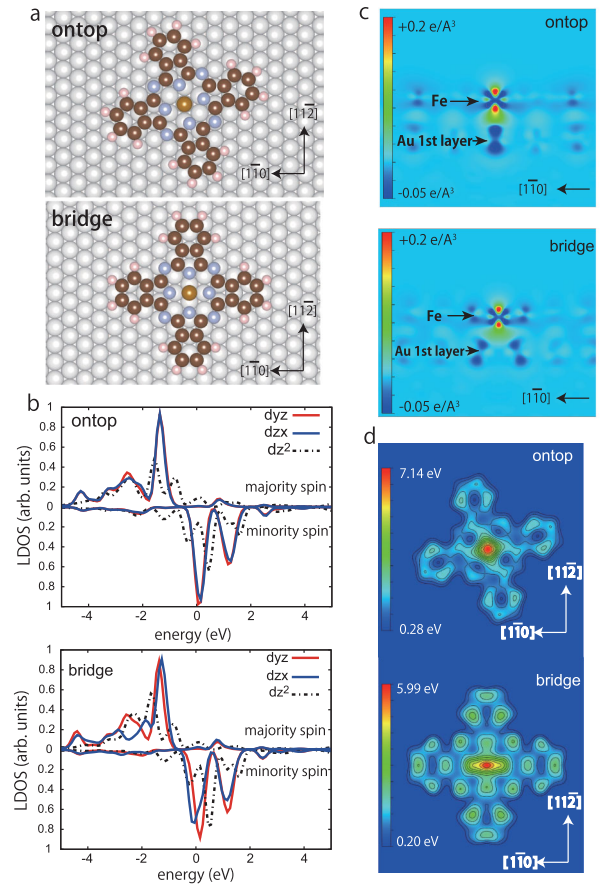


FIG. 2 (color). (a) The optimized structures of on top and bridge species on Au(111). (b) Spin-polarized local density of states (SP-LDOS) projected on the d_{zx} , d_{yz} and d_{z^2} orbitals of Fe. The upper and lower panels show the SP-LDOS calculated for the on top and bridge species, respectively. The d_{zx} and d_{yz} orbitals for the on top species overlap each other. (c) The cross section of the differential charge distribution $[\Delta\rho(r)]$ for both species. (d) The differential local potential distribution $[\Delta V_{\text{loc}}(r)]$ for both species. Panels (a), (c), and (d) are rendered by VESTA [37].

d_π orbitals in isolated FePc survives for the on top species while it is lifted for the bridge species.

The difference in the d_π orbitals of both species comes from the local symmetry of the adsorption site. To clarify this, we carried out a calculation of the differential charge distribution ($\Delta\rho(r) = \rho_{\text{tot}}(r) - \{\rho_{\text{sub}}(r) + \rho_{\text{mol}}(r)\}$) and differential local potential distribution ($\Delta V_{\text{loc}}(r) = V_{\text{loc}}^{\text{total}}(r) - \{V_{\text{loc}}^{\text{sub}}(r) + V_{\text{loc}}^{\text{mol}}(r)\}$). $\rho_{\text{tot}}(V_{\text{loc}}^{\text{total}})$ is the charge density (local potential [22]) of the molecule-adsorption system, and $\rho_{\text{sub}}(V_{\text{loc}}^{\text{sub}})$ and $\rho_{\text{mol}}(V_{\text{loc}}^{\text{mol}})$ are those of the surface and a free molecule, respectively. $\Delta\rho(r)$ and the $\Delta V_{\text{loc}}(r)$ clearly demonstrate the bonding nature and the symmetry [Figs. 2(c) and 2(d)]. The cross section of $\Delta\rho(r)$ of the on top species shows that the bond is formed mainly by the hybridization of the d_{z^2} orbital with the Au atom beneath [Fig. 2(c)]. As a result, fourfold symmetry is kept locally around the Fe atom as shown in [Fig. 2(d)]. The holding of fourfold symmetry allows degeneracy of the d_π orbitals, resulting in the survival of the orbital degrees of freedom as reported by the x-ray magnetic circular dichroism work [21]. The bonding charges are distributed between the Fe atom and the two nearest-neighbor Au atoms for the bridge species [Fig. 2(c)], reducing the local symmetry of the ligand field to the twofold one [Fig. 2(d)]. This symmetry difference between the on top and bridge configurations is not clearly resolved in Fig. 1(a) because the topographic STM image reflects the contributions from the Fe 3d states and the ligand states. The characteristic distribution localized around the Fe atom may be blurred.

The *ab initio* calculations also provide an answer to the puzzling competition between the Kondo effect and zero field splitting (ZFS) in FePc on Au(111). ZFS lifts the degeneracy in the spin sublevels to suppress the Kondo correlations. For a half-integer spin system, the Kondo effect coexists with ZFS in the case that the sublevels of $S_z = \pm 1/2$ are the ground state [10,32]. However, in the integer spin systems with ZFS, the Kondo effect is unlikely to occur because the spin degeneracy in the ground state needed for the Kondo effect is removed. FePc is a typical example of an integer spin with ZFS ($S = 1$ and a ZFS of 8.7 meV between the $S_z = 0$ and $S_z = \pm 1$ sublevels [33]). ZFS also remains in FePc on a surface [34]. Thus, the Kondo effect is not expected to occur for FePc on Au(111). The Kondo signature emerging against this expectation comes from the different coupling strength of the d_{z^2} and d_π orbitals with the substrate. The stronger coupling of the d_{z^2} orbital enhances T_K to 100 ~ 200 K, which surpasses the energy scale of ZFS. Thus, as the temperature is lowered, the first Kondo screening arises before ZFS becomes dominant. Then, the effective Hamiltonian to describe the system at the lower temperature regime, below several K, falls into the Kondo type with $S = 1/2$ rather than ZFS.

Following the first Kondo screening, the localized electron in the d_π orbitals which weakly couple with the

substrate is screened in the second stage. The second-stage Kondo screening is observed for the on top species as a sharp dip while it is not for the bridge species. The difference comes from the degeneracy of the d_π orbitals preserved only for the on top species. Both spin and orbital degrees of freedom are available for the screening; i.e., the SU(4) Kondo channels open for the on top species. In contrast, only the SU(2) channels are available for the bridge species due to the reduced symmetry. Compared to the SU(2) Kondo effect, the SU(4) Kondo temperature, $T_K^{\text{SU}(4)}$, is enhanced by the increase in the number of screening channels [35] so that the second-stage Kondo effect appears only for the on top species. The second-stage Kondo signature cannot be observed for the bridge species because $T_K^{\text{SU}(2)}$ is much lower than $T_K^{\text{SU}(4)}$.

To confirm this model, we calculated $T_K^{\text{SU}(4)}$ and $T_K^{\text{SU}(2)}$ by NRG method based on the electronic structure derived from the LDA + U calculations [28]. Increasing the energy separation between the d_{zx} and d_{yz} orbitals (τ), the degeneracy is removed and then the crossover from the SU(4) to the SU(2) Kondo effect occurs. When $T_K^{\text{SU}(4)} = 2.7\text{K}$, $T_K^{\text{SU}(2)}$ goes down to 0.2 K at $\tau = 100$ meV, which is merged into the background at the experimental temperature (0.4 K). This supports the two-stage Kondo effect and the dependence of the Kondo signature on the adsorption symmetry.

The SU(4) Kondo effect for the on top species is supported furthermore by the magnetic-field evolution of the dip. FePc on Au(111) has both an orbital and spin magnetic moment so that the single particle energy level of the d_π electron ($E_{m\sigma}$) shifts due to the spin and orbital Zeeman effects under a magnetic field. Since the orbital magnetic moment parallel to the molecular plane (m_L^{xy}) is much larger than the perpendicular one [21], the energy shift due to the orbital Zeeman effect is larger for the parallel magnetic field, leading to a dependence of the Kondo spectrum on the direction of the magnetic field. $E_{m\sigma}$ can be written as $E_{m\sigma} = E_0 + \Delta_{\text{orb}}(\delta_{m,1} - \delta_{m,-1}) + \frac{\Delta_{\text{spin}}}{2}(\delta_{\sigma,1} - \delta_{\sigma,-1})$ with $\Delta_{\text{orb}} = -m_L^{xy}|\vec{B}_\parallel|\mu_B$ and $\Delta_{\text{spin}} = -gm_S|\vec{B}_\parallel|\mu_B$, where B_\parallel is the in-plane component of the magnetic field, m_S is the spin magnetic moment, μ_B is the Bohr magneton, and $g = 2.0$ is the Landé g factor. The subscript m is a magnetic quantum number to specify the degenerate d_π orbitals, and δ is the Kronecker delta function. Figures 3(a) and 3(b) show the spectral evolution of the Kondo dip with magnetic fields perpendicular and parallel to the molecular plane (denoted by B_\perp and B_\parallel), respectively. The dip is gradually quenched by increasing B_\perp from 0 to 6 T without splitting. In contrast, the shoulder appears at $B_\parallel = 2$ T. As B_\parallel increases, the dip splits and the splitting becomes larger with the gradual quenching of the spectral intensity. To rationalize these features, the magnetic field evolution of the single particle energy spectrum was calculated by NRG, including the magnetic field effect through $E_{m\sigma}$. In the NRG calculation, we set $m_S = m_L^{xy} = 0.5\mu_B$.

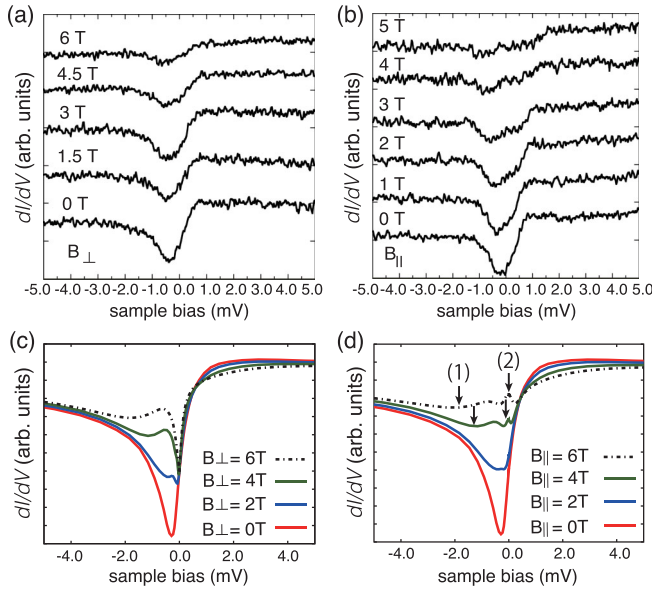


FIG. 3 (color). The evolution of STS spectra under external magnetic fields (a) B_{\perp} and (b) B_{\parallel} , respectively. These spectra were taken at ~ 0.7 K with $V_{\text{rms}} = 0.06$ mV and 312.6 Hz by keeping the STM tip over the Fe atom. The spectra were not changed basically when the orientation of magnetic field was rotated within the molecular plane. The spectral evolutions calculated by NRG at 0 K as a function of the magnetic field (c) B_{\perp} and (d) B_{\parallel} , respectively.

The NRG calculation shows that the dip evolves into a broad structure and a sharp dip with the increase of B_{\perp} [Fig. 3(c)]. The broad structure and the sharp dip stem from the excitation associated with the spin-Zeeman effect and the SU(2) orbital Kondo effect, respectively. The spin-Zeeman splitting by B_{\perp} causes the crossover from the SU(4) to the SU(2) orbital Kondo regime so that the sharp dip becomes narrower with an increase of magnetic fields. The estimated T_K is 1.4 and 1 K at $B_{\perp} = 4$ T and 6 T, respectively. Therefore, the dip is not observed clearly due to the thermal broadening at the experimental temperature (0.7 K). The spectral intensity near E_F remains due to the SU(2) orbital Kondo effect and thus the dip is not split clearly but it shows up as a broad single dip. The NRG calculation for B_{\parallel} [Fig. 3(d)] shows that the dip splits into a broad dip [marked by (1) in Fig. 3(d)] and fine structure [marked by (2) in Fig. 3(d)] around E_F at $B_{\parallel} = 4$ T due to the symmetry breaking caused by both spin and orbital Zeeman effects. Considering that the fine structure around E_F appears as a broad structure in the STS spectra, the spectral variation observed in Fig. 3(b) is reasonably reproduced by the NRG calculation. A similar spectral dependence on the orientation of the magnetic field is observed for the SU(4) Kondo effect in the carbon-nanotube QD [20], which is a universal signature of the SU(4) Kondo effect.

Finally, we examine another interpretation of the above spectral feature. The spin SU(2) Kondo effect combined with

a strong anisotropy in the Landé g factor might explain the magnetic field direction dependence. In the spin SU(2) Kondo effect, the Kondo resonance is split by the spin Zeeman effect when the Zeeman energy is comparable to T_K [36]. If the perpendicular component of the g factor is smaller than the parallel components, the magnetic field at which the splitting occurs is larger in the perpendicular direction than in the parallel direction, which causes the dependence on the direction of the magnetic field. One important characteristic of this model is that the quenching of the Kondo resonance must always be accompanied by splitting. In contrast to this, the dip is quenched without splitting, as shown in Fig. 3(a). Therefore, the SU(2) Kondo effect with a strong anisotropy in the g factor can be ruled out.

This work was partially supported by the Japan Society for the Promotion of Science (JSPS) through Grant-in-Aid for Research Activity Start-up (23860070) and by the Ministry of Education, Science, Sports, and Technology (MEXT) Grant-in-Aid for Scientific Research (21241027, 21225001, and 22760026). N. T. thanks the support from the Asahi Glass Foundation. The calculations were performed by using the computer facilities of Kyushu University Research Institute for Information Technology, the Institute of Solid State Physics (ISSP Super Computer Center, the University of Tokyo), and the RIKEN Integrated Cluster of Clusters (RICC) facility.

*n-takagi@k.u-tokyo.ac.jp

- [1] J. Kondo, *Prog. Theor. Phys.* **32**, 37 (1964).
- [2] A. C. Hewson, *The Kondo Problem to Heavy Fermions* (Cambridge University, Cambridge, England, 1993).
- [3] D. Goldhaber-Gordon, H. Shtrikman, D. Mahalu, D. Abusch-Magder, U. Meirav, and M. A. Kastner, *Nature (London)* **391**, 156 (1998).
- [4] S. M. Cronenwett, T. H. Oosterkamp, and L. P. Kouwenhoven, *Science* **281**, 540 (1998).
- [5] S. Sasaki, S. D. Franceschi, J. M. Elzerman, W. G. van der Wiel, M. Eto, S. Tarucha, and L. P. Kouwenhoven, *Nature (London)* **405**, 764 (2000).
- [6] S. Sasaki, S. Amaha, N. Asakawa, M. Eto, and S. Tarucha, *Phys. Rev. Lett.* **93**, 017205 (2004).
- [7] J. Li, W.-D. Schneider, R. Berndt, and B. Delley, *Phys. Rev. Lett.* **80**, 2893 (1998).
- [8] V. Madhavan, W. Chen, T. Jamneala, M. F. Crommie, and N. S. Wingreen, *Science* **280**, 567 (1998).
- [9] H. P. Manoharan, C. P. Lutz, and D. M. Eigler, *Nature (London)* **403**, 512 (2000).
- [10] A. F. Otte, M. Ternes, K. von Bergmann, S. Loth, H. Brune, C. P. Lutz, C. F. Hirjibehedin, and A. J. Heinrich, *Nature Phys.* **4**, 847 (2008).
- [11] J. Park *et al.*, *Nature (London)* **417**, 722 (2002).
- [12] W. Liang, M. P. Shores, M. Bockrath, J. R. Long, and H. Park, *Nature (London)* **417**, 725 (2002).
- [13] A. Zhao *et al.*, *Science* **309**, 1542 (2005).
- [14] L. Gao *et al.*, *Phys. Rev. Lett.* **99**, 106402 (2007).
- [15] J. J. Parks *et al.*, *Science* **328**, 1370 (2010).

- [16] N. Tsukahara, S. Shiraki, S. Itou, N. Ohta, N. Takagi, and M. Kawai, *Phys. Rev. Lett.* **106**, 187201 (2011).
- [17] K. J. Franke, G. Schulze, and J. I. Pascual, *Science* **332**, 940 (2011).
- [18] P. Jarillo-Herrero, J. Kong, H. S. J. van der Zant, C. Dekker, L. P. Kouwenhoven, and S. De Francesch, *Nature (London)* **434**, 484 (2005).
- [19] M.-S. Choi, R. López, and R. Aguado, *Phys. Rev. Lett.* **95**, 067204 (2005).
- [20] A. Makarovski, A. Zhukov, J. Liu, and G. Finkelstein, *Phys. Rev. B* **75**, 241407 (2007).
- [21] S. Stepanow, P. S. Miedema, A. Mugarza, G. Ceballos, P. Moras, J. C. Cezar, C. Carbone, F. M. F. de Groot, and P. Gambardella, *Phys. Rev. B* **83**, 220401 (2011).
- [22] G. Kresse and J. Furthmüller, *Phys. Rev. B* **54**, 11169 (1996).
- [23] G. Kresse and J. Furthmüller, *Comput. Mater. Sci.* **6**, 15 (1996).
- [24] P. E. Blöchl, *Phys. Rev. B* **50**, 17953 (1994).
- [25] S. L. Dudarev, G. A. Botton, S. Y. Savrasov, C. J. Humphreys, and A. P. Sutton, *Phys. Rev. B* **57**, 1505 (1998).
- [26] E. Minamitani, D. Matsunaka, N. Tsukahara, N. Takagi, M. Kawai, and Y. Kim, *e-J. Surf. Sci. Nanotechnol.* **10**, 38 (2012).
- [27] We use the exchange-correlation functional, determined by D. M. Ceperley and B. J. Alder, *Phys. Rev. Lett.* **45**, 566 (1980), and parameterized by J. P. Perdew and A. Zunger, *Phys. Rev. B* **23**, 5048 (1981).
- [28] See Supplemental Material at <http://link.aps.org/supplemental/10.1103/PhysRevLett.109.086602> for supplementary texts and figures.
- [29] U. Fano, *Phys. Rev.* **124**, 1866 (1961).
- [30] H. Kasai, W. A. Diño, and A. Okiji, *Surf. Sci. Rep.* **43**, 1 (2001).
- [31] E. Minamitani, W. A. Diño, H. Nakanishi, and H. Kasai, *Surf. Sci.* **604**, 2139 (2010).
- [32] R. Žitko, R. Peters, and T. Pruschke, *Phys. Rev. B* **78**, 224404 (2008).
- [33] B. W. Dale, R. J. P. Williams, C. E. Johnson, and T. L. Thorp, *J. Chem. Phys.* **49**, 3441 (1968).
- [34] N. Tsukahara *et al.*, *Phys. Rev. Lett.* **102**, 167203 (2009).
- [35] J. S. Lim, M.-S. Choi, M. Y. Choi, R. López, and R. Aguado, *Phys. Rev. B* **74**, 205119 (2006).
- [36] T. A. Costi, *Phys. Rev. Lett.* **85**, 1504 (2000).
- [37] K. Momma and F. Izumi, *J. Appl. Crystallogr.* **41**, 653 (2008).